Performance enhancement of $SnSb_2Se_3S$ solar cells through structural and optoelectronic modifications

U.K. Anjali, M. Irshad Ahamed, and J. Abdul Raashid

Department of Electronics and Communication Engineering, E.G.S. Pillay Engineering College, Nagapattinam – 611002, Tamilnadu, India.

E. Edward Anand

Department of Science and Humanities, E.G.S. Pillay Engineering College, Nagapattinam – 611002, Tamilnadu, India.

Received 14 July 2025; accepted 28 August 2025

This study investigates the optoelectronic properties of $SnSb_2Se_3S$, a novel material, for the first time, and evaluates its potential as a high-absorption thin-film solar cell absorber. Leveraging its unique nanoscale attributes and potential for Multiple Exciton Generation (MEG), $SnSb_2Se_3S$ is explored for its capacity to enhance light absorption and charge carrier transport, positioning it as a promising candidate for advanced photovoltaic applications. A detailed analysis of Power Conversion Efficiency (PCE) as a function of absorber layer thickness demonstrates a direct correlation, with PCE values increasing from 5.87% at 2500 nm to 5.96% at 3000 nm. The impact of electron affinity on PCE is also examined, revealing an inverse relationship wherein increased electron affinity results in decreased efficiency due to alterations in charge transport dynamics. Furthermore, the temperature dependence of PCE is analyzed, indicating robust stability across a range of operating temperatures. Quantum Efficiency (QE) measurements show a significant response at 1240 nm, confirming effective infrared absorption. The carrier generation rate is evaluated, confirming efficient photon-to-electron conversion within the absorber layer. These results provide critical insights into the viability of $SnSb_2Se_3S$ as an alternative absorber material for next-generation solar cells, setting the stage for subsequent experimental validation and device optimization.

Keywords: Solar cells; SCAPS-1D; optoelectronics; $SnSb_2Se_3S$.

DOI: https://doi.org/10.31349/RevMexFis.72.011602

1. Introduction

Globally, the demand for different kinds of energy is surging due to population growth and the economic and industrial advancement of developing countries. Consumption of energy is still largely dependent on fossil fuels. However, due to increasing environmental concerns, the world needs to shift towards renewable energy sources [1, 2]. According to Oil & gas journal's report [3], at the beginning of 2025 global oil consumption was estimated to hover around 104 million barrels per day, whereas natural gas supplies over 60% of the world's electricity. At the same time, renewable energy is gaining momentum: solar and wind capacity extensions are on track to surpass approximately 400GW this year [4], storage battery installations are on the rise, and green pilot projects are flourishing. These indicate a clear shift toward cleaner energy even as the world navigates steadily rising fossil fuel demand [5]. In light of this, extensive research and development efforts have been devoted to solar energy technology.

In general, solar technology falls into two categories: photovoltaic (PV) and concentrating solar power (CSP). Photovoltaic convert sunlight into electricity via the photoelectric effect, utilizing materials, notably silicon, with conductive properties. Conversely, in CSP technologies, lenses or mirrors are used to concentrate sunlight, and they are generally viable for large-scale deployments [6]. While solar power generation is inherently intermittent and subject to geographical and temporal variations, it often correlates well with daily energy consumption.

A solar cell or PV cell is an energy harvesting technology. It facilitates solar energy conversion directly into electricity. PV cell is typically made with a semiconducting material and is capable of absorbing more photons from sunlight to creating an excitation of electrons from the semiconductor surface [7]. The generation of electric current takes place when the cell is connected to an external circuit with separate electrons flowing from one side to the other. Direct current (DC) electricity is produced by this flow of electrons. As the charges start moving and they accumulate at the terminals, a potential difference (voltage) is established in the circuit [8].

The band gap of a PV cell determines how efficiently it converts light into electricity. A semiconductor with an appropriate band gap can absorb a large portion of the solar spectrum. And their bandgap allows both reasonable current and voltage — leading to maximum power output. This makes semi conducting materials ideal for use in photovoltaic cells as light-absorbing materials [9, 10]. In solar cell manufacturing, thin films are very beneficial due to their thickness, cost effectiveness, flexibility and easy to manufacture on large scales. Solar cells of the future will benefit from thin film semiconductors, since they are highly desirable owing to their energy efficiency, scalability, and superior spectral utilization [11–13].

Within the landscape of semiconductor materials under investigation for solar cell applications, quaternary compounds are distinguished by their exceptional tunability of optical and electrical properties, which makes them highly promising materials for next-generation photovoltaic applications [14, 15]. The strategic combination of quaternary materials in diverse compositions and layered architectures enables the fabrication of solar cells capable of capturing a broader spectral spectrum, thus advancing the frontiers of solar technology towards enhanced efficiencies and expanded application versatility. As research in this domain advances, quaternary materials are poised to play a pivotal role in the development of innovative materials for advanced renewable energy applications, contributing significantly to a sustainable energy future. In this context, we hypothesize that $SnSb_2Se_3S$, as a novel quaternary material, will demonstrate promising photovoltaic performance due to its favourable bandgap, strong absorption, and efficient charge transport properties, as revealed through SCAPS-1D simulations.

In this study, the quaternary compound $SnSb_2Se_3S$ is investigated as an absorber layer for photovoltaic. By analysing on the individual photovoltaic performance of tin and antimony, we theoretically justify their inclusion in the quaternary chalcogenide compounds [16–18]. Utilizing SCAPS-1D simulation software, the optoelectronic performance of this material is evaluated, elucidating its potential and limitations for effective solar cell implementation. In steady-state conditions, SCAPS-1D solves coupled Poisson and continuity equations for electrons and holes. In our $SnSb_2Se_3S$ model, we input realistic values for electron affinity, bandgap, carrier mobility, and defect levels based on data available for Sb_2Se_3 and similar Sn-based compounds [19, 20]. A first-level performance prediction can be made using this approximation. The distinct optoelectronic properties and sustainable attributes of antimony-based compounds contribute significantly to photovoltaic technology [21]. The tunable band gaps of materials such as Sb_2Se_3 and $SnSb_2Se_3S$, coupled with their strong absorption in the visible and near-infrared spectral regions [22], facilitate efficient solar energy conversion. Their quasi-one-dimensional crystal structures promote efficient charge transport and minimize carrier recombination, while also imparting flexibility, a desirable trait for next-generation flexible photovoltaic. $SnSb_2Se_3S$, a quaternary semiconductor composed of tin (Sn), antimony (Sb), selenium (Se), and sulphur (S), benefits from the strategic incorporation of sulphur and selenium, which play a critical role in bandgap engineering and enhancement of photovoltaic performance, as observed in analogous quaternary compounds [23, 24]. Simulations conducted under standard AM 1.5G illumination (100 mW/cm^2) yielded significant performance metrics, including short-circuit current density (J_{sc}), power conversion efficiency (η), open-circuit voltage (V_{oc}), and fill factor (FF).

This study investigates the photovoltaic performance of a solar cell, focusing on the influence of key operational parameters on efficiency. The current–voltage characteristics of solar cells with $SnSb_2Se_3S$ absorber layers were investigated, revealing that a thickness of 2500 nm and above begins to deliver favourable simulation results. Based on this observation, selected thicknesses up to 3000 nm were analysed to assess their impact on power conversion efficiency (PCE).Furthermore, the temperature dependence of PCE is analysed across a range of 240 K to 340 K, providing insights into the device's thermal stability and performance variations. To elucidate the light absorption characteristics, the generation rate of photo generated carriers as a function of depth within the absorber layer is evaluated, quantifying the efficiency of photon absorption at various depths within the material.

Furthermore, this study evaluates the impact of the CdS buffer layer's electron affinity on device performance by comparing results obtained with values of 4.0 eV and 4.215 eV, thereby assessing its influence on current-voltage ($J-V$) characteristics and charge transport dynamics. A sensitivity analysis can be carried out by selecting these two values to measure the effect of slight deviations in electron affinity (within a physically meaningful range) on key parameters. The correlation between the absorption coefficient of the absorber material and the fill factor under illumination is also examined, revealing the influence of material properties on photovoltaic cell performance. Additionally, quantum efficiency (QE) is analysed to determine the optimal wavelength range for maximizing the photovoltaic response of the cell. Through these comprehensive investigations, a thorough understanding of the critical factors governing solar cell efficiency and performance is sought.

2. Simulation methodology

Computational modeling, known for its efficiency and cost-effectiveness in evaluating solar cell performance through systematic input variation, was applied in this study using SCAPS-1D due to its proven reliability in simulating solar cell behavior.

SCAPS-1D numerically solves semiconductor equations under steady-state conditions within a one-dimensional framework, employing Poisson's and continuity equations to model charge transport [25]. Specifically, Poisson's equation, which governs the relationship between space charge density (ρ) and the electric field (E) within a heterojunction, is utilized and can be expressed as follows:

2.1. Poisson's equation

$$\frac{d^2\Psi}{dx^2} = -\frac{q}{\varepsilon}(p - n + N_D^+ - N_D^-). \tag{1}$$

In this equation Ψ is electrostatic potential, q is elementary charge, N_D is the density of ionized donor ions, N_A identifies the density of ionized acceptors, and p and n are hole and electron densities.

In a semiconductor device, the continuity equations describe the transport and recombination of charge carriers (electrons and holes) as shown in Eqs. (2) and (3).

2.2. Electron continuity equation

$$\frac{dn}{dt} = \frac{1}{q}\frac{dJ_n}{dx} + G - R. \tag{2}$$

2.3. Hole continuity equation

$$\frac{dp}{dt} = -\frac{1}{q}\frac{dJ_p}{dx} + G - R. \tag{3}$$

Current densities of electrons and holes are J_n and J_p, while generation and recombination rates are G and R, respectively.

To describe charge carrier flow, SCAPS-1d uses drift-diffusion transport equations [26, 27], they are given by the Eqs. (4) and (5).

$$J_n = qn\mu_n E + qD_n, \tag{4}$$

and

$$J_p = qp\mu_p E - qD_p\frac{dp}{dx}, \tag{5}$$

According to Eqs. (4) and (5), μ_n is the electron mobility, μ_p is the hole mobility, D_n and D_p are the electron and hole diffusion coefficients, q is the charge, and E is the electric field. By solving these equations, SCAPS-1D effectively models solar cell performance, calculates essential parameters, and facilitates device design optimization for improved efficiency.

These fundamental semiconductor equations are material-independent [28], which means that the simulation can handle binary, ternary, and quaternary semiconductors as long as the right material parameters (bandgap, dielectric constant, mobility, electron affinity, absorption coefficient, etc.) are provided. In order to determine the parameters of the proposed quaternary material $SnSb_2Se_3S$ either experimental reports were obtained when available, or trends from related materials were used to estimate the parameters. Even though the SCAPS software is not atomistic in nature, its physical model is valid for device-level analysis of semiconductors when parameter estimation and validation are taken into account. This approach ensures that the mathematical and physical framework used in SCAPS remains applicable and reliable for simulating the photovoltaic behaviour of the quaternary compound $SnSb_2Se_3S$.

3. Theoretical parameters and structural design

The input parameters of the simulation for solar cell structures Ag/$SnSb_2Se_3S$/CdS/ZnSe/FTO are outlined in Table I. The absorber layer parameters are theoretically calculated, while other parameters are taken from relevant literature [29, 30].

The schematic structure of the Ag/$SnSb_2Se_3S$/CdS/ZnSe /FTO solar cell comprises a p-type $SnSb_2Se_3S$ absorber layer, which serves as the primary light-absorbing material. This is followed by a buffer layer of n-type CdS, which facilitates charge carrier separation and minimizes interface recombination losses. Additionally, an n-type ZnSe electron transport layer (ETL) is incorporated for efficiently extracting and transporting electrons to the front electrode. The device is completed with an Ag contact as the back electrode and a transparent conductive layer of FTO (Fluorine-doped Tin Oxide), ensuring efficient light transmission and charge collection.

4. Results and discussion

This investigation centres on evaluating the efficiency of the quaternary compound $SnSb_2Se_3S$ as an absorption layer for photovoltaic applications. Utilizing SCAPS-1D simulation software, a systematic analysis of $SnSb_2Se_3S$'s performance as an absorber layer was conducted to ascertain its potential and limitations. This analysis encompassed the evaluation of critical parameters, including absorber layer thickness and

TABLE I. Physical parameters of different layers used in the simulation.

Settings	Absorber $SnSb_2Se_3S$	Buffer layer CdS	Intermediate layer ZnSe
Thickness (nm)	2500	1000	10
Band gap energy (eV)	4.0	2.45	2.9
Affinity (eV)	2.97	4.215	4.0
Dielectric permittivity (relative)	10	10	10
State densities in CB, N_c (cm^{-3})	2.2×10^{18}	2.2×10^{18}	2.2×10^{18}
State densities in VB, N_v (cm^{-3})	1.8×10^{19}	9.1×10^{18}	1.8×10^{19}
Electron speed Ve(cm/s)	1.1×10^{7}	1×10^{7}	1×10^{7}
Hole speed, V_h (cm/s)	6.4×10^{6}	1×10^{7}	1×10^{7}
Electron mobility μ_n (cm^2/V·s)	10	1×10^{2}	50
Hole mobility μ_p (cm^2/V·s)	5	2.5×10^{1}	20

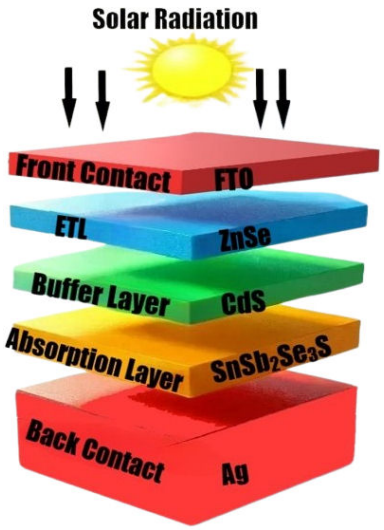

FIGURE 1. Schematic structure of simulation device.

temperature variations, and their combined impact on key photovoltaic performance metrics such as open-circuit voltage (V_{oc}), short-circuit current density (J_{sc}), fill factor, and overall efficiency.

4.1. Impact of absorption layer thickness

The thickness of the absorption layer significantly influences various aspects of solar cell performance, including photon absorption, charge carrier collection, and overall efficiency. Increasing layer thickness enhances photon absorption and charge carrier generation. However, this can also result in increased recombination losses and diminished carrier collection, particularly in materials with low mobility. Conversely, a thinner layer minimizes recombination but may compromise light absorption, thus limiting performance. The optimal thickness is determined by balancing light absorption and carrier transport, considering the material's absorption coefficient [31, 32]. In this study, $SnSb_2Se_3S$ is employed as the absorption layer. A thin-film solar cell with an absorber layer thickness ranging between 2500 and 3000 nm was selected to achieve strong photovoltaic performance. The current density-voltage (J–V) characteristics for varying absorption layer thicknesses, ranging from 2500 nm to 3000 nm, are presented in Fig. 2.

The results show a clear correlation between absorber layer thicknesses and short-circuit current density (J_{sc}). Simulations revealed that performance begins to improve from 2500 nm, as this thickness enables more effective absorption of incident light, enhancing charge carrier generation. The simulated J–V curve of the $SnSb_2Se_3S$ solar cell displays typical diode-like behaviour, with V_{oc}=0.2265 V and J_{sc} = 48.586 mA/cm^2, resembling the trend reported by Dursun *et al*. [33]. Despite strong optical absorption, the relatively low efficiency is attributed to recombination losses and suboptimal band alignment at the CdS interface. The smooth curve highlights a low fill factor, and the results represent a conservative estimate based on theoretical parameters. This behavior aligns with findings by Ammar Shahib *et al*. [34], who also observed increases in J_{sc} and V_{oc} with greater absorber thickness. In this study, a 2500 nm layer yielded $J_{sc} = 48.415$ mA/cm^2 and $V_{oc} = 0.2232$ V, which improved to J_{sc} = 48.586 mA/cm^2 and V_{oc} = 0.2265 V at 3000 nm. These trends were confirmed through repeated simulations, supporting the conclusion that thicker absorber layers can enhance photovoltaic performance.

Figures 3 and 4 illustrate the impact of absorption layer thickness on current density and voltage, respectively. As depicted, both current density and voltage exhibit distinct positive correlations with increasing layer thickness.

This trend underscores the critical role of thicker absorber layers in enhancing photon absorption and charge carrier generation, thereby contributing to improved device efficiency [35]. Conversely, Fig. 5 demonstrates an inverse relationship between absorption layer thicknesses, wherein FF decreases with increasing thickness. The observed decrease in Fill Factor (FF) with increasing absorption layer thickness highlights the intricate interplay between light absorption,

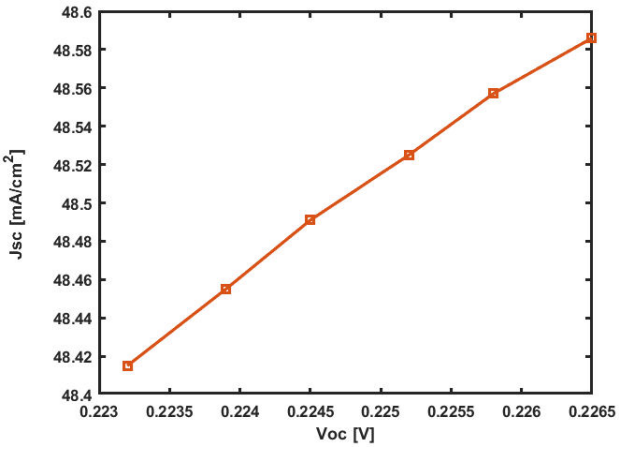

FIGURE 2. Current density vs voltage.

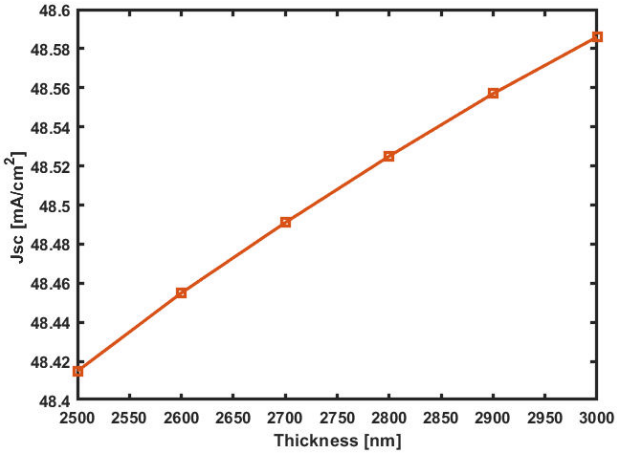

FIGURE 3. Thickness (nm) vs J_{sc} mA/cm^2.

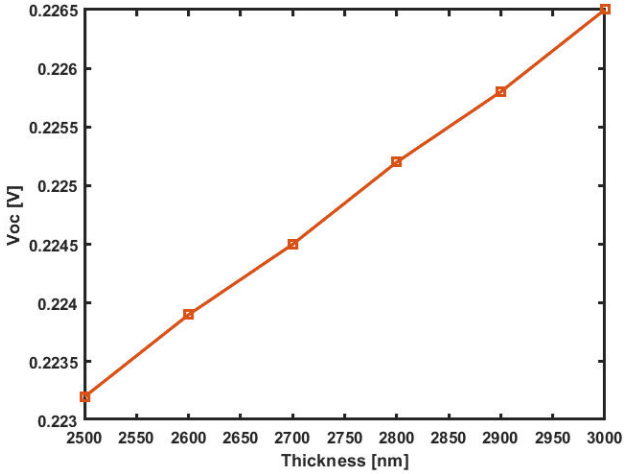

FIGURE 4. Thickness (nm) vs voltage V.

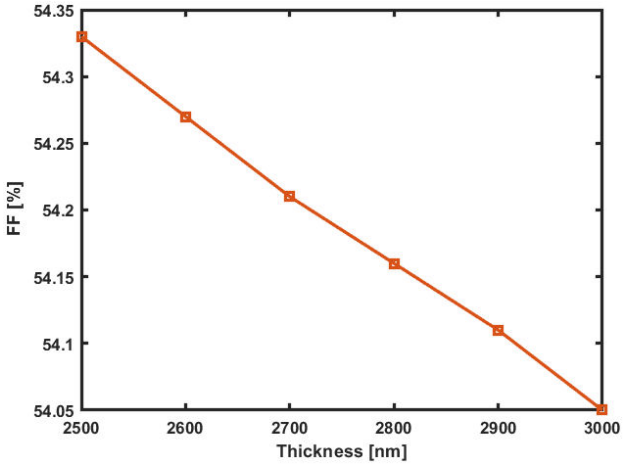

FIGURE 5. FF (%) vs Thickness (nm).

charge carrier transport, and resistive losses. Specifically, this study revealed an FF of 54.33% at a 2500 nm absorber layer thickness, which subsequently decreased to 54.05% at 3000 nm.

When the diffusion length is shorter than the layer thickness, charge carriers recombine before reaching the electrodes, leading to reduced current collection and consequently, a lower FF [36–38].

Notably, recent research by Himadri Sekar Das *et al*. reported similar trends, demonstrating an increase in J_{sc} and V_{oc} with absorber layer thickness, accompanied by a concurrent decrease in FF. The results obtained in the present study, as depicted in Fig. 5, align consistently with the findings reported in Ref. [39].

4.2. Temperature's influence on power conversion efficiency

An increase in temperature leads to a reduction in the semiconductor's bandgap, primarily due to thermal vibrations within the crystal lattice. These vibrations weaken interatomic bonding forces, facilitating electron transitions between the valence and conduction bands [40]. This study investigates the temperature dependence of power conversion efficiency (PCE) for $SnSb_2Se_3S$, utilizing an absorber layer thickness of 2500 nm across a temperature range of 240 K to 340 K. The results, as depicted in Fig. 6, reveal a pronounced inverse relationship between temperature and PCE. Specifically, PCE decreases significantly from 9.01% at 240 K to 4.04% at 340 K, demonstrating a clear temperature-dependent performance characteristic.

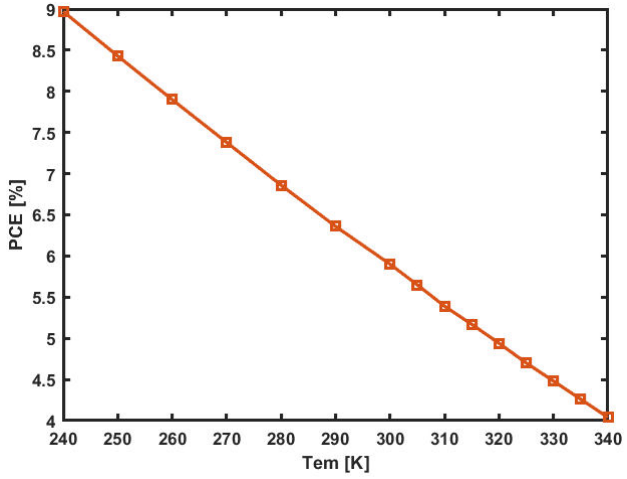

FIGURE 6. Temperature Vs PCE %.

The simulated $SnSb_2Se_3S$ solar cell shows a decrease in power conversion efficiency (PCE) with increasing temperature. This is mainly due to a reduction in open-circuit voltage (V_{oc}), which follows the relation:

$$V_{oc} = \frac{kT}{q} \ln\left(\frac{J_{sc}}{J_o} + 1\right), \tag{6}$$

where, V_{oc} = open-circuit voltage, k is Boltzmann constant, T is absolute temperature K, q is elementary charge, J_{sc} is short-circuit current density and J_o is reverse saturation current density.

From the equation, as the temperature rises, the reverse saturation current J_o increases exponentially, causing a logarithmic drop in V_{oc}. Additionally, elevated temperatures enhance recombination through defect states in the absorber and at interfaces, common in multinary compounds [41] like $SnSb_2Se_3S$. Increased thermal energy can also reduce carrier mobility and raise series resistance, leading to a drop in fill factor. Together, these effects contribute to the decline in PCE at higher temperatures.

A similar temperature-dependent trend has been reported by Segbefia [42], where increasing temperature led to a decline in V_{oc}, fill factor, and overall solar cell efficiency — consistent with the results observed in the present study. Conversely, a reduction in temperature improves V_{oc} and enhances device performance. As outlined in *Theory of Solar Cells* [43], higher temperatures contribute to greater recombination and thermal losses, which reduce PCE, while lower temperatures are beneficial due to minimized losses and a slight widening of the bandgap. These findings reinforce the

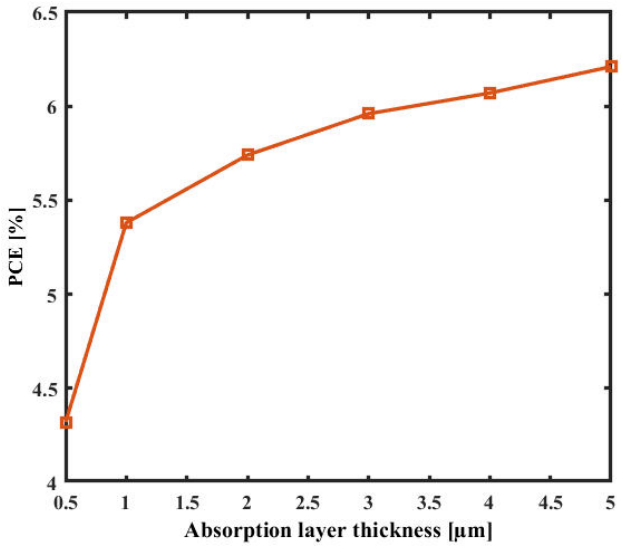

FIGURE 7. PCE (%) Vs. Absorption layer thickness (μm).

thermal sensitivity of the $SnSb_2Se_3S$ absorber and confirm the robustness of its efficiency behaviour under varying thermal conditions.

4.3. Overall performance of PCE (%) vs thickness and temperature

Figure 7 shows the overall PCE characteristics of the device with an absorption layer ranging from 10 to 5000 nanometres thick. The Power Conversion Efficiency (PCE) of the device increases significantly with absorber layer thickness, rising from 0.4% at 10 nm to 6.21% at 5000 nm. In extremely thin layers, light absorption is minimal, resulting in low carrier generation and poor efficiency. As thickness increases, absorption improves rapidly, leading to a sharp rise in PCE—reaching 5.38% at 1000 nm. However, beyond this point, the rate of improvement slows, with PCE increasing only slightly to 6.21% at 5000 nm. This nonlinear behaviour is due to absorption approaching saturation and the growing impact of recombination losses and transport limitations in thicker films. This trend underscores the direct correlation between absorber layer thickness and light absorption capability, which subsequently enhances device performance.

Table II presents the detailed PCE values (%) for various absorber layer thicknesses.

TABLE II. Thickness and its PCE values.

S. No	Absorption layer thickness (μm)	PCE %
1	0.01	0.4
2	0.5	4.32
3	1	5.38
4	2	5.74
5	3	5.96
6	4	6.07
7	5	6.21

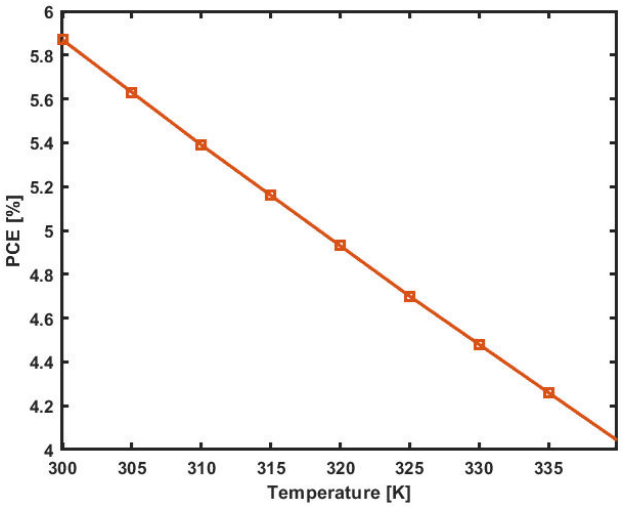

FIGURE 8. PCE vs temperature.

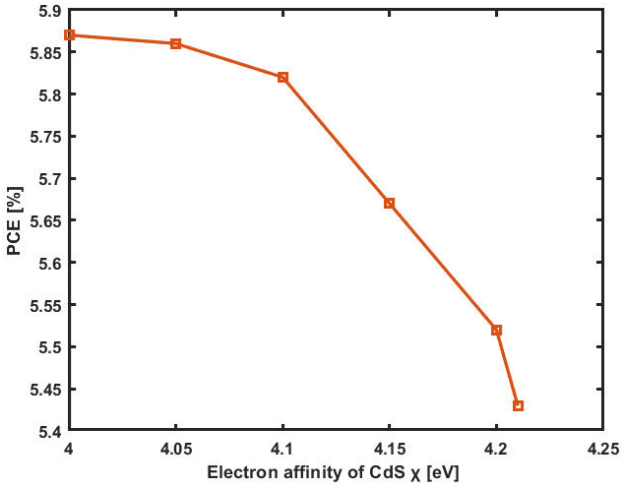

FIGURE 9. PCE vs Electron Affinity of CdS.

The analysis of PCE percentages for the given material across various temperatures shows a declining linear trend with increasing absorber layer thickness. PCE values decreases from 5.9% at 300 K to 3.9 % at 340 K. Figure 8 shows the change in PCE values at different temperatures.

The impact of CdS electron affinity on Power Conversion Efficiency (PCE) is illustrated in Fig. 9, revealing a trend of decreasing PCE values with increasing electron affinity. This observation aligns with findings reported by Avijit Talukdar *et al*. [44], who attributed the decline in PCE to a reduction in the energy offset between the absorption and transport layers. Specifically, an elevated electron affinity weakens the built-in electric field, thereby impeding carrier separation and transport, and consequently diminishing PCE.

The observed decrease in Power Conversion Efficiency (PCE) with increasing electron affinity indicates that while higher electron affinity may optimize energy level alignment, it can also introduce challenges related to charge transport

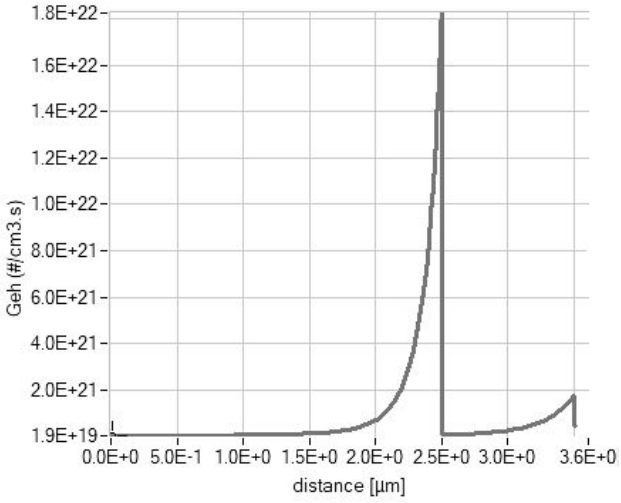

FIGURE 10. Geh vs depth.

and collection. This presents an opportunity for targeted material optimization. Specifically, improvements in surface passivation and a reduction in recombination losses could enhance charge collection and, consequently, elevate PCE. Through meticulous adjustment of material properties, overall device performance can be significantly improved, leading to the development of more efficient solar cells.

4.4. Carrier generation rate vs depth

Figure 10 shows how light is absorbed within a solar cell and where most electron-hole pairs are generated within the material, as measured by the rate of carriers generated by photons through the absorb layer. The analysis of photogenerated carrier generation rate (Geh) revealed a stable value of 1.9×10^{19} cm^{-3} up to a depth of 2.0 μm. beyond this point, Geh exhibited a gradual increase, culminating in a peak value of 1.8×10^{22} cm^{-3}. This pronounced peak, observed within the 2.0 μm to 2.5 μm depth range, signifies optimal incident light absorption and, consequently, maximum photogenerated carrier generation. This phenomenon indicates an optimal interaction between the material's optical absorption coefficient and the incident light intensity within this specific region. Beyond 2.5 μm, the Geh value returned to a constant level of 1.9×10^{19} cm^{-3}, persisting until 3.0 μm. A minor increase in Geh was noted beyond 3.0 μm, suggesting residual light absorption within the absorber layer at this depth. This slight increase may also be attributed to numerical approximations or assumptions inherent in certain computational models, including considerations for carrier diffusion or field effects.

4.5. Current density vs voltage with different electron affinity of CdS

CdS electron affinity is typically measured in the range 4.0 eV to 4.5 eV depending on factors such as material quality, synthesis method and measurement techniques. In this

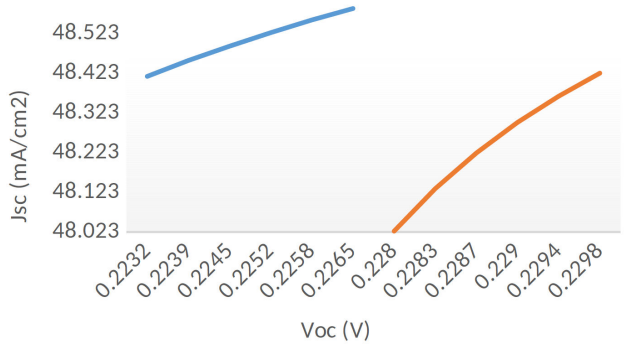

FIGURE 11. J_{sc} vs V_{oc}.

TABLE III. J_{sc} vs V_{oc} performance with electron affinity values of CdS.

CdS electron affinity (eV)	Voltage (V) x-axis	Current density y-axis
4.215	0.2280	48.025
4.00	0.2232	48.415

study, we selected 4.0 eV and 4.215 eV to represent two commonly reported and realistic values. These values help us understand how small changes in electron affinity can affect the performance of $SnSb_2Se_3S$-based solar cells, especially in terms of $J-V$ characteristics and charge transport at the CdS interface. Figure 11 shows how CdS's electron affinity affects the $J-V$ performance of solar cells based on $SnSb_2Se_3S$.

This study revealed that at an electron affinity of 4.0 eV, the open-circuit voltage V_{oc} was notably low, measuring 0.2232 V, while the short-circuit current density J_{sc} was comparatively high, at 48.415 mA/cm^2. A slight increase in the CdS electron affinity to 4.215 eV resulted in a marginal increase in V_{oc}, reaching 0.2280 V, accompanied by a slight decrease in J_{sc}, which measured 48.025 mA/cm^2. These corresponding values are summarized in Table III.

This observed trend is attributable to alterations in the band alignment at the interface. A lower electron affinity creates a larger conduction band offset, which elevates the energy barrier for electron transport, thereby reducing voltage. However, it also strengthens the built-in electric field, enhancing carrier extraction and consequently leading to a higher current density [45]. These results underscore the inherent trade-off between V_{oc} and J_{sc} when adjusting CdS electron affinity, emphasizing the critical need for precise band alignment optimization to achieve improved solar cell efficiency.

4.6. Influence of absorption coefficient on fill factor

Figure 12 illustrates the relationship between the solar cell's electrical performance and its light-absorbing efficiency. Here, as the absorption coefficient increases, the fill factor decreases.

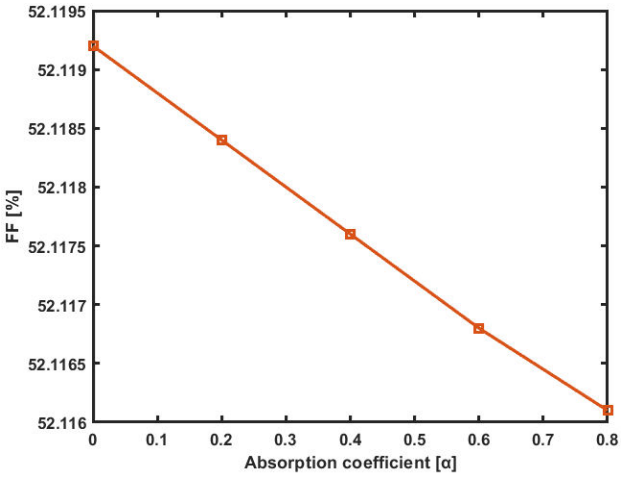

FIGURE 12. Absorption coefficient vs fill factor.

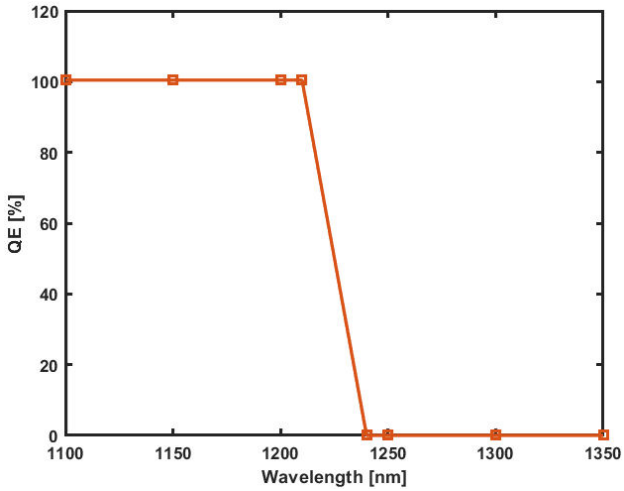

FIGURE 13. QE vs wavelength (nm).

This inverse relationship suggests that materials exhibiting high absorption coefficients may be susceptible to increased recombination or compromised charge transport. Strong surface absorption can exacerbate recombination losses, particularly in the presence of inadequate passivation or suboptimal interface properties. Furthermore, rapid absorption can limit carrier generation within deeper regions of the material, thereby reducing charge collection efficiency [46]. Consequently, enhancing the absorption coefficient must be coupled with concurrent optimization of material quality and charge transport characteristics to ensure a high fill factor in solar cells.

4.7. Quantum efficiency vs wavelength

Figure 13 illustrates the QE response of the $SnSb_2Se_3S$ solar cell across the wavelength spectrum, showing a notable QE peak of 100.04% at 1240 nm.

This value exceeding 100% strongly suggests the occurrence of Multiple Exciton Generation (MEG) in the material. MEG is a quantum process wherein a single high-energy photon generates multiple electron-hole pairs, thereby increasing the number of charge carriers contributing to the photocurrent.

This effect typically arises when the photon energy exceeds twice the material's bandgap, allowing excess energy—normally lost as heat through thermalization—to instead create additional excitons. In the case of $SnSb_2Se_3S$, the photon energy around 1240 nm ($\sim$ 1 eV) aligns closely with the material's absorption edge, creating favourable conditions for MEG.

This observation is consistent with the findings of Octavi E. Semonin *et al*. [47] in their study, *Peak external photocurrent quantum efficiency exceeding 100% via MEG in a quantum dot solar cell*, where MEG was identified as the mechanism behind QE surpassing 100%. They demonstrated that quantum dots enabled efficient utilization of photon energy through MEG, thereby enhancing solar cell performance.

And R.S Sahu *et al*. (2022) [48] reported similar behavior in VO_2, where strong electronic interactions enhanced EQE up to 160%, confirming that MEG can occur in diverse semiconductors beyond quantum dots.

The presence of MEG in $SnSb_2Se_3S$ highlights the material's potential for enhanced carrier multiplication, making it particularly promising for high-efficiency, low-bandgap solar cell applications, especially where near-infrared light harvesting is critical.

Future studies will focus on experimentally validating the MEG effect observed in simulations, using advanced optical and electrical characterization techniques. Additionally, optimizing interface engineering and exploring quantum-confined versions of $SnSb_2Se_3S$ may further enhance MEG activity and carrier dynamics. Incorporating MEG-aware modeling and tandem architectures could provide deeper insight into the fundamental photophysical behaviour of this material and its potential for next-generation photovoltaic applications.

5. Conclusion

A simulation-based analysis of the Ag/$SnSb_2Se_3S$/CdS/ZnSe /FTO solar cell structure was conducted using SCAPS-1D software to investigate its photovoltaic performance. The study examined the influence of absorption layer thickness, CdS buffer layer electron affinity, and operating temperature on device characteristics. While the fill factor decreased with increasing absorber layer thickness, the power conversion efficiency (PCE) exhibited a positive correlation, attributed to an increase in short-circuit current density J_{sc} and improved open-circuit voltage V_{oc}. Variation in CdS electron affinity yielded V_{oc} and J_{sc} values of 0.2232 V and 48.415 mA/cm^2 at 4.0 eV and 0.2280 V and 48.025 mA/cm^2 at 4.215 eV, respectively, highlighting the sensitivity of device performance to this parameter. The photogenerated carrier generation rate peaked at 1.8×10^{22} cm^{-3}·s^{-1} at a depth of 2.5 μm, with a subsequent minor increase to 2.1×10^{21} cm^{-3}·s^{-1} at 3.6 μm.

Notably, the quantum efficiency (QE) reached 100.44% at 1240 nm, indicative of Multiple Exciton Generation (MEG). The material's strong infrared absorption and high efficiency under low-light conditions suggest its suitability for applications such as portable solar chargers, contributing to the enhancement of solar-powered device performance and the advancement of sustainable energy solutions.

1. Q. Hassan *et al*., The renewable energy role in the global energy *Transformations*, **48** (2024) 100545, https://doi.org/10.1016/j.ref2024.100545
2. I. Ahamed *et al*., Investigation of thermal evaporated SnSe nano structure layer for photovoltaic use: a structural, morphological, and electrical analysis, *J Mater Sci: Mater Electron* **36** (2025) 224, https://doi.org/10.1007/s10854-025-14299-9
3. M. Al-Moneef and E. Yousef, Global Oil Demand Outlook: Trends and Implications, Global Oil Demand Outlook: Trends and Implications. *Oil & Gas Journal* **123** (2025) 45.
4. E. Graham, N. Fulghum, and K. Altieri, Global Electricity Review 2025 (ember-energy.org, 2025), https://ember-energy.org/app/uploads/2025/04/Report-Global-Electricity-Review-2025.pdf.
5. Q. Hassan *et al*., The renewable energy role in the global energy Transformations, *Renewable Energy Focus* **48** (2024) 100545, https://doi.org/10.1016/j.ref.2024.100545
6. L. Yao *et al*., Evaluating the feasibility of concentrated solar power as a replacement for coal-fired power in China: A comprehensive comparative analysis, *Applied Energy* **377** (2025) 124396, https://doi.org/10.1016/j.apenergy.2024.124396
7. N. S. Seroka, R. Taziwa, and L. Khotseng, Solar energy materials-evolution and Niche applications: A literature review, *Materials* **15** (2022) 5338, https://doi.org/10.3390/ma15155338
8. M. Pavlik *et al*., Analysis and evaluation of photovoltaic cell defects and their impact on electricity generation, *Energies* **16** (2023) 2576, https://doi.org/10.3390/en16062576
9. G. Jarosz, R. Marczy'nski, and R. Signerski, Effect of band gap on power conversion efficiency of single-junction semiconductor photovoltaic cells under white light phosphor-based LED, *illumination* **107** (2019) 104812, https://doi.org/10.1016/j.mssp.2019.104812
10. P. J. S. Babu *et al*., Studies on copper indium selenide/Zinc sulphide semiconductor quantum dots for solar cell applications, *Chalcogenide Letters*. **18** (2021) 701, https://chalcogen.ro
11. S. M. Sivasankar, C. de Oliveira Amorim, and A. F. da Cunha, Progress in Thin-Film Photovoltaics: A Review of Key Strategies to Enhance the Efficiency of CIGS, CdTe and CZTSSe Solar Cells, *J. Compos. Sci*. **9** (2025) 143, https://doi.org/10.3390/jcs9030143
12. J. Liu *et al*., Evolutionary manufacturing approaches for advancing flexible perovskite solar cells, *Joule* **8** (2024) 944, https://doi.org/10.1016/j.joule.2024.02.025
13. A. R. Smith *et al*., Thin-Film Technologies for Sustainable Building-Integrated Photovoltaics, *Energies* **17** (2024) 6363, https://doi.org/10.3390/en17246363
14. K. N'Konou, S. Y. Kim, and N. Y. Doumon, Multicomponent organic blend systems: A review of quaternary organic photovoltaics, *Carbon & Energy* **6** (2024) e579, https://doi.org/10.1002/cey2.579
15. A. K. Yadav *et al.*, Cu2SrSnS4 absorber based efficient heterostructure single junction solar cell: a hybrid- DFT and macroscopic simulation studies, *Appl. Phys. A* **130** (2024), https://doi.org/10.1007/s00339-023-07184-x
16. X. Wang *et al*., Band Versus: Charge Transport in Antimony Chalcogenides, *ACS Energy Lett.* **7** (2022) 2954, https://doi.org/10.48550/arXiv.2206.15389
17. U. A. Shah *et al*., A deep dive into Cu2ZnSnS4 (CZTS) Solar cells: A review of exploring roadblocks, Breakthroughs & shaping the future, *Small* **20** (2024) 2310584, https://doi.org/10.1002/smll.202310584
18. M. I. Ahamed *et al.*, Modelling of Cu2SnSeS chalcogenide quantum dots for optoelectronic applications, *Journal of optoelectronics and advanced materials* **25** (2023) 169.
19. P. Kumar *et al*., Progress in Sb2Se3 and Sb2S3-Based Solar Cells: SCAPS-1D and Experimental Investigations, *Chemistry Select* **10** (2025) e202404430, https://doi.org/10.1002/slct.202404430
20. K. K. M. Mamta and V. N. Singh, Sb2Se3 as an HTL for Mo/Sb2Se3/Cs2TiF6/TiO2 solar structure: performance evaluation with SCAPS-1D, *Heliyon* **8** (2022) e10925, https://doi.org/10.1016/j.heliyon.2022.e10925
21. G. Chen *et al.*, Perspective of Environmentally friendly antimony Selenide-based solar cell, *Appl. Phys. Lett.* **125** (2024) 200502, https://doi.org/10.1063/5.0214349
22. M. Wang *et al.*, Suppressing material loss in the visible and near-infrared range for functional Nano photonics using bandgap engineering, *Nat Commun.* **11** (2020) 5055, https://doi.org/10.1038/s41467-020-18793-y
23. T. Taskesen *et al*., Steep sulfur gradient in CZTSSe solar cells by H2S-assisted rapid surface sulfurization, *RSC Adv.* **11** (2021) 12687, https://doi.org/10.1039/ D1RA00494H
24. S. Mohammadi, N. Kaur, and D. R. Radu, Nanoscale Cu2ZnSnSxSe(4-x) (CZTS/Se) for Sustainable Solutions in Renewable Energy, Sensing, and Nano medicine, *Crystals* **14** (2024) 479, https://doi.org/10.3390/cryst14050479
25. M. Burgelman, P. Nollet, and S. Degrave, Modelling polycrystalline semiconductor solar cells, *Thin Solid Films* **361-362** (2000) 527, https://doi.org/10.1016/S0040-6090(99)00825-1

26. M. Rahaman *et al.*, Numerical optimization of lead-based and lead-free absorber materials for perovskite solar cell (PSC) architectures: A SCAPS-1D simulation, *AIP Advances* **14** (2024), https://doi.org/10.1063/5.0217486

27. T. Sekou *et al*., Comparative Analysis Using SCAPS-1d Software on the stability and toxicity of the Perovskites FAPbI 3 , and FASI 3, *Advances Energy Conversion Materials* **308** (2024), https://doi.org/10.37256/aecm.5220245549

28. M. Burgelman and S. D. P Nollet, Modelling polycrystalline semiconductor solar cells, *Thin Solid Films* **361-362** (2000) 527, https://doi.org/10.1016/S0040-6090(99)00825-1

29. P. G. D. K. Ngue *et al.*, Investigation of the Performance of a Sb2S3-Based Solar Cell with a Hybrid Electron Transport Layer (h-ETL): A Simulation Approach Using SCAPS-1D Software, International Journal of Photoenergy **2024** (2024) 5188636, https://doi.org/10.1155/2024/5188636

30. A. El Khalfi *et al.*, Dual-Absorber Solar Cell Design and Simulation Based on Sb2Se3 and CZTGSe for High-Efficiency Solar Cells, *Langmuir* **40** (2024) 20352, https://doi.org/10.1021/acs.langmuir.4c01472

31. T. Ahamed *et al*., Numerical Modelling of Buffer Layers for Advancing CZTSSe Solar Cell Efficiency (2025), URL https://arxiv.org/abs/2501.06681.

32. S. Wang *et al*., Corrigendum to Enhanced performance of TiO2-based perovskite solar cells with Ru-doped TiO2 electron transport layer Sol, *Energy* **169** (2018) 335, https://doi.org/10.1016/j.solener.2020.06.082

33. S. Dursun, J-V and C-V characteristic of CdS/CdTe solar cell modelled by SCAPS-1D program (2022), https://doi.org/10.5281/zenodo.7472259.

34. A. Shahib *et al*., Modelling of Highly Efficient Copper Zinc Tin Sulphide (CZTS) Solar cell for Performance Improvement (2019), https://dx.doi.org/10.1109/ICECCE47252.2019.8940765.

35. M. Noman, A. D. Khan, and S. T. Jan, Influence of Absorber Layer Thickness and Band Gap Tuning on the Optical and Electrical Properties of Semi-transparent Flexible Perovskites Solar Cells (GREEN ENERGY AND TECHNOLOGY, 2024), https://doi.org/10.1007/978-3-031-49787-2_3.

36. M. Saladina and C. Deibel, Transport resistance strikes back: unveiling its impact on fill factor losses in organic solar cells (2024), https://doi.org/10.48550/arXiv.2404.06190

37. M. S. Reza *et al*., Design and Optimization of High- Performance Novel RbPbBr3-Based Solar Cells with Wide- Band-Gap S-Chalcogenide. Electron Transport Layers (ETLs), *ACS Omega* **9** (2024) 19824, https://doi.org/10.1021/acsomega.3c08285

38. Y. Osman *et al*., Optimized CIGS-Based Solar Cell Towardsan Efficient solar cell: Impact of layers Thickness and doping (Optical and Quantum Electronics, 2021), https://link.springer.com/article/10.1007/s11082-021-02873-4

39. H. S. Das *et al*., Effect of Absorber Layer Thickness on the Performance of the Perovskite Solar Cell in Solar Cell Capacitance Simulator-1D (SCAPS-1D), *ES Gen.* **6** (2024), https://dx.doi.org/10.30919/esg1292

40. Y. Cho *et al*., Temperature dependence on bandgap of semiconductor photo catalysts, *J. Chem. Phys*. **152** (2020) 231101, https://doi.org/10.1063/5.0012330

41. L. M. Shaker *et al*., Examining the influence of thermal effects on solar cells: a comprehensive review, *Sustainable Energy Research* **11** (2024) 6, https://doi.org/10.1186/s40807-024-00100-8

42. O. K. Segbefia, Temperature profiles of field-aged photovoltaic modules affected by optical degradation, *Heliyon* **9** (2023) e19566, https://doi.org/10.1016/j.heliyon. 2023.e19566

43. L. M. Shaker *et al*., Examining the influence of thermal effects on solar cells: a comprehensive review, *Sustainable Energy Res.* **11** (2024), https://doi.org/10.1186/s40807-024-00100-8

44. A. Talukdar *et al*., Unveiling the role of band offset in inorganic RbGeI3-based perovskites solar cells: a numerical study in SCAPS-1D, *Indian Journal of Physics* **98** (2024) 3913, https://link.springer.com/article/10.1007/s12648-024-03158-8

45. D. Valenta *et al*., The Energy Level Alignment at the Buffer/Cu (In, Ga) Se2 Thin-Film Solar Cell Interface for CdS and GaOx, *Advanced Materials Interfaces* **11** (2024) 2301110, https://doi.org/10.1002/admi.202301110

46. L. M. M. Livingston *et al*., Impact of Device Design Parameters on Quantum Efficiency of Solar Cells and Revelation of Recombination Mechanism, *Optical and Quantum Electronics* **57** (2025) 160, https://doi.org/10.1007/s11082-025-08074-7

47. O. E. Semonin *et al.*, Peak external photocurrent quantum efficiency exceeding 100% via MEG in a quantum dot solar cell, *Science (New York, N.Y.)* **334** (2011) 1530, https://pubmed.ncbi.nlm.nih.gov/22174246/

48. S. R. Sahu *et al*., Multiple exciton generation in VO2, *Phys. Rev. B* **108** (2023) 125133, https://doi.org/10.1103/PhysRevB.108.125133